Superficies y Vacío ***9****, 193-198, Diciembre 1999*

Excimer laser treated Ag/Co multilayers exhibiting giant magnetoresistance effect

M. Jergel, A. Anopchenko, E. Majková, M. Spasova, Š. Luby
Institute of Physics of the Slovak Academy of Sciences, Dúbravská cesta 9, 842 28 Bratislava, Slovakia,

V. Holý
Laboratory of Thin Films and Nanostructures, Masaryk University, Kotlárská 2, 611 37 Brno, Czech Republic

M. Brunel
Laboratoire de Cristallographie du CNRS, B.P.166, 38042 Grenoble Cedex 09, France

A. Luches, M. Martino
I.N.F.M. and University of Lecce, Department of Physics, 73100 Lecce, Italy

An interplay between the structure and giant magnetoresistance (GMR) in laser treated Ag/Co multilayers (MLs) is studied. Three samples with different Ag layer thicknesses, denoted according to nominal values (in nm) as Ag_2Co_1, Ag_4Co_1, and Ag_6Co_1, were exposed to XeCl excimer laser pulses of the fluences (0.1-0.25) Jcm^{-2} for (1-200) times. The structure was examined by X-ray diffraction, hard X-ray reflectivity, and diffuse scattering measurements at grazing incidence. The polycrystalline face-centered cubic structure of Ag layers with random orientation of the grains was found in as-deposited Ag_2Co_1 and Ag_6Co_1. The formation of a discontinuous ML by grain boundary diffusion of Ag into Co layers induced by laser treatment is evidenced in Ag_6Co_1 which explains a systematic increase of the GMR up to the melting threshold for Ag layers. The temperature window for diffusion is too narrow for completing such a process in Ag_2Co_1. A strong texture of Ag layers found in Ag_4Co_1 stabilizes the as-deposited structure and prevents from a systematical increase of the GMR. When the Ag melting threshold is reached, the ML structure is lost and rapid solidification results into a granular-like structure, independent of the structure of the original ML. This structure need not be optimal for achieving a high GMR value.

1. Introduction

A lot of effort has been devoted to an enhancement of the giant magnetoresistance (GMR) effect in multilayers (MLs) by a post-deposition thermal treatment. To our knowledge, a laser optimization of the GMR has been absent in the literature though it has more advantages. It enables us to deposit a required amount of energy into the volume of a thin film without heating the substrate.

This amount is controlled by two independent parameters – fluence and number of pulses. Recently, we have started the studies of the effect of excimer laser irradiation on the GMR in Ag/Co MLs[1,2]. We have found that below the melting threshold for Ag layers, the GMR may be enhanced more than twice provided the temperature window for diffusion is large enough.

The enhancement of the GMR was supposed to be due to the formation of a discontinuous ML. The formation of such discontinuous MLs with enhanced GMR was reported for some traditionally annealed MLs[3-5]. In this work, we concentrate on interplay between the GMR results obtained previously[1,2] and the underlying structural changes induced by excimer laser annealing. Though it is hard to get a direct evidence of a discontinuous ML formation, there is a possibility of investigating it via interface morphology evolution.

Therefore, a complex structural study of Ag/Co MLs is performed including the interface sensitive X-ray reflectivity (XRR) and diffuse scattering at grazing incidence (GIDS) measurements.

2. Experimental

The samples were prepared by electron-beam evaporation onto Si(100) wafers covered by a 300 nm thick SiO_2. The vacuum prior and during the deposition was 10^{-7} Pa and 10^{-6} Pa, respectively. Three MLs of nominal parameters (2 nm Ag/1 nm Co)x5, (4 nm Ag/1 nm Co)x10, (6 nm Ag/1 nm Co)x5 were deposited starting with Ag. They are labelled further as Ag_2Co_1, Ag_4Co_1, Ag_6Co_1, respectively.

The thermal treatment was performed by excimer XeCl laser with laser fluences F=0.1, 0.15, 0.20, 0.25 Jcm^{-2}. The laser pulses were repeated n=1, 10, 20, 50, 100, 200 times with the frequency of 10 Hz, the pulse duration being 30 ns. Numerical calculations were applied to find the temperature time and depth evolutions as described in Ref. 6. For the fluences used and the repetition frequency of 10 Hz, the laser pulses are thermally independent

Therefore the total deposited energy is proportional to the number of pulses for a given fluence. Both Co (T_{melt}=1768 K) and Ag (T_{melt}=1235 K) layers melt at the fluence F=0.25 Jcm^{-2} while Co layers remain solid for $F \leq 0.2$ Jcm^{-2}. Ag layers melt at F=0.15 Jcm^{-2} for Ag_2Co_1 and Ag_4Co_1 MLs while for Ag_6Co_1 ML, they melt for the fluence F=0.25 Jcm^{-2} only. If Ag layers melt, they melt in the whole depth of MLs.

The atomic structure of MLs was examined by X-ray diffraction (XRD) measured both in the symmetrical (Bragg-Brentano - BB) and asymmetrical (grazing incidence - GI) modes using CuK_α radiation.

The BB XRD was measured on a commercial powder diffractometer with
a focusing graphite monochromator placed in the secondary beam and a scintillation NaI(Tl) detector. The GI XRD was measured on a laboratory-made diffractometer with a primary beam graphite monochromator. A curved 120° position sensitive detector and a 12 kW rotating anode X-ray generator decreased the acquisition time considerably. The characterization of the ML stack and interfaces was obtained from the XRR and GIDS measurements. They were performed on a high-resolution diffractometer equipped with double-crystal GaAs monochromator using $CuK_{\alpha 1}$ radiation.

The GMR ratio was calculated as $[R(H)–R(50kOe)]/R(50kOe)$ where $R(H)$ is the electrical resistance measured as a function of the magnetic field applied parallel or perpendicular to the sample surface. Further details may be found in our previous works[1,2].

3. Results

The GI XRD patterns of as-deposited Ag_2Co_1 and Ag_6Co_1 MLs taken at the angle of incidence a=0.5° are shown in Fig.1. Both MLs exhibit a complete set of diffraction maxima of the face-centered cubic (fcc) Ag phase. Moreover, the maximum labeled as A may point at the presence of a small fraction of hexagonal close-packed (hcp) ordering (203 diffraction). Co diffraction maxima are not seen due to the small thickness of Co layers and a low scattering power of Co atoms

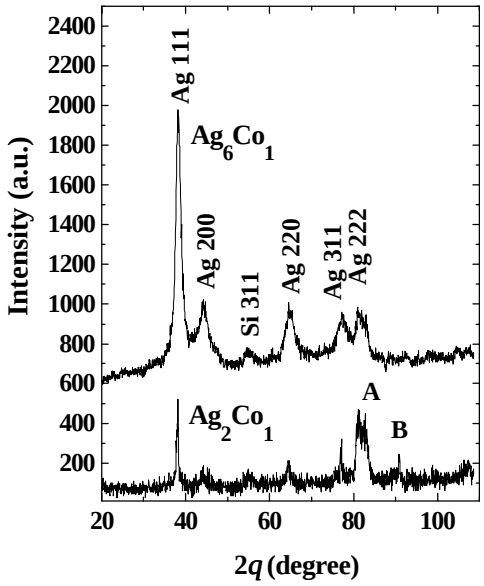

Fig. 1. X-ray diffraction patterns taken at grazing incidence of 0.5° for as-deposited Ag_2Co_1 and Ag_6Co_1 MLs. The curve for the latter is shifted upwards. 2q is the angle between the primary and secondary beams. The diffractions A and B are discussed in the text. Si 311 diffraction comes from the substrate.

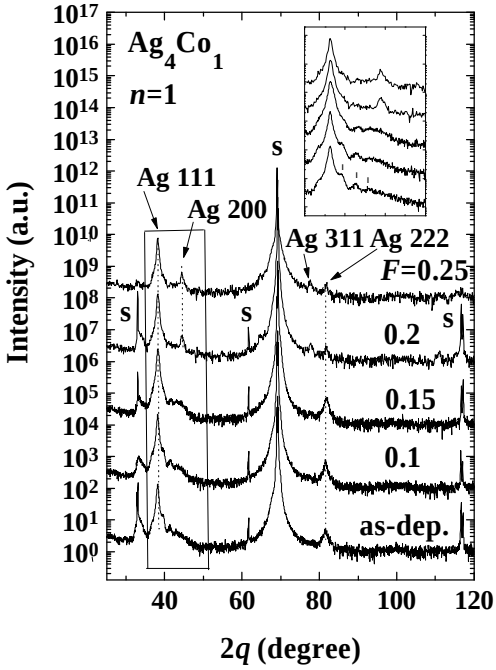

Fig. 2. X-ray diffraction patterns taken in Bragg-Brentano geometry before and after one pulse irradiation with different fluences for Ag_4Co_1 ML. The curves for laser treated samples are shifted upwards. 2q is the angle between the primary and secondary beams. The superlattice satellites around Ag 111 diffraction are shown in more detail in the inset. The diffractions coming from the substrate are labeled as «s».

Moreover, 200 diffraction of the fcc Ag phase partially overlaps with a strong 002 diffraction of the hcp Co phase..Thus only the maximum labeled as B may point at the tendency to hcp ordering in Co layers (200 diffraction). The polycrystalline structure of fcc Ag with random orientation of grains persists in Ag_2Co_1 and Ag_6Co_1 MLs also after the laser annealing at F=0.2 Jcm^{-2}. The presence of only distinct Ag diffractions after laser irradiation is in accordance with the immiscibility of Ag and Co following from the phase diagram. The BB XRD pattern of as-deposited Ag_4Co_1 ML shows only 111 and 222 diffractions of fcc Ag (Fig.2). Moreover, the satellites around 111 diffraction are recognizable. As the scattering vector is kept perpendicular to the sample surface in BB mode, these features hint at a strongly textured (superlattice-like) structure with (111) planes in Ag grains oriented preferentially parallel to the surface. From the positions of the satellites of 111 diffraction, the ML period of ≈5 nm is calculated and from its integral width, the size of coherently scattering domains of 26 nm is found which covers ≈5 ML periods. For F=0.1 Jcm^{-2}, the strongly textured structure is preserved up to n=200. For F=0.15 Jcm^{-2}, it is gradually lost with increasing n. The satellites disappear and another 200 diffraction of fcc Ag emerges from the background. For F=0.2 Jcm^{-2}, further Ag diffractions appear and the superlattice satellites are absent.

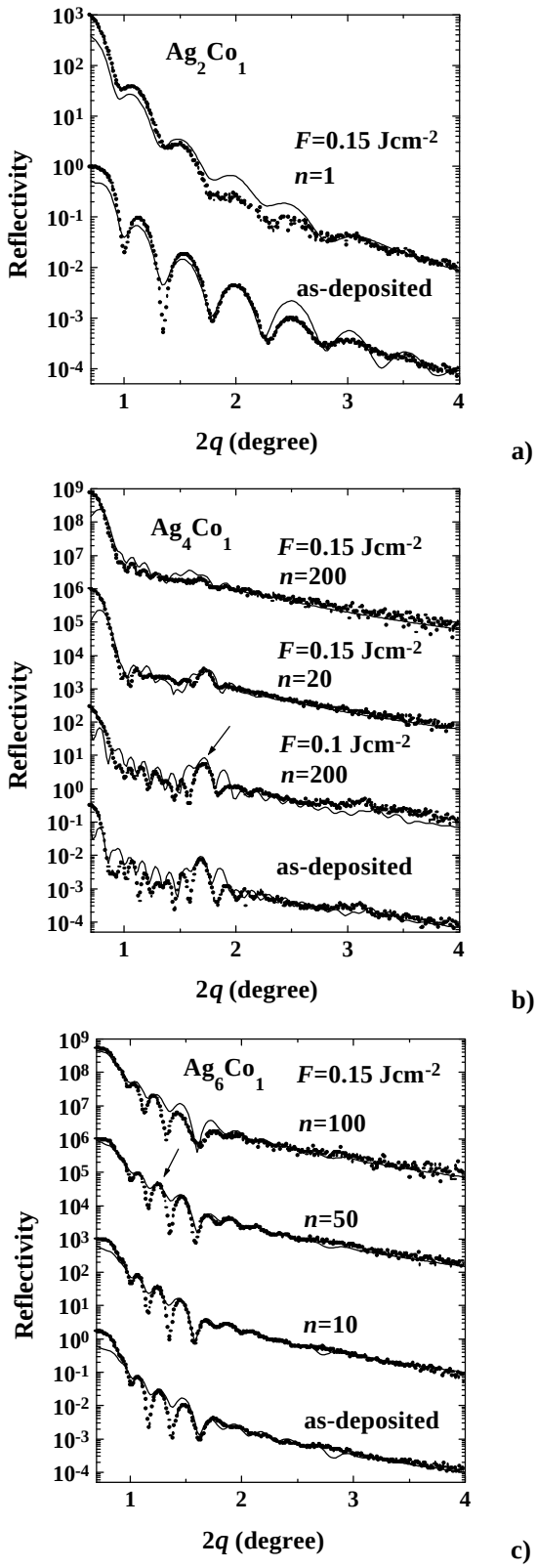

Fig. 3. Evolution of specular XRR with laser annealing for (a) Ag_2Co_1 (b) Ag_4Co_1, and (c) Ag_6Co_1 MLs. The measured curves (dots) were simulated by Fresnel optical computational code (line) and for laser treated samples they are shifted upwards. 2*q* is the angle between the primary and secondary beams. For the meaning of the arrows see Fig.4.

The specular XRR curves of as-deposited MLs as well as their evolution after F=0.15 Jcm^{-2} irradiation are shown in Fig.3. For as-deposited Ag_4Co_1 ML, the most distinct maximum comes from the ML period (the 1st Bragg maximum) while the smaller ones are connected with the total thickness of the ML stack (so called Kiessig maxima).

The existence of two kinds of maxima points to a rather regular ML structure in the as-deposited Ag_4Co_1 ML. It is not observed in two other as-deposited MLs because of a smaller number of ML periods. Ag_2Co_1 ML is heavily damaged after one pulse irradiation at F=0.15 Jcm^{-2} while for Ag_4Co_1 ML it is the case only for n=200. For F=0.1 Jcm^{-2} and n=200, Ag_4Co_1 ML is rather untouched. Ag_6Co_1 ML exhibits pronounced XRR modulations at F=0.15 Jcm^{-2} for all n values as well as for F=0.2 Jcm^{-2} and n=20. The XRR curves were simulated using the Fresnel optical computational code[7] to extract the basic ML parameters.

Their evolution with laser treatment is documented in Table I. The period of as-deposited Ag_4Co_1 ML is consistent with the value assessed from the satellites around Ag 111 diffraction. The interface roughness s was included into simulations by a Debye-Waller-like attenuation factor corresponding to the error function interface profile. However, the XRR measurements are sensitive to the projection of the interface profiles into the perpendicular direction only (direction of the scattering vector) so that they cannot reveal lateral interface characteristics.

To characterize the interface morphology, GIDS measurements with a non-zero lateral (along the interfaces) component of the scattering vector are unavoidable. We traced the distribution of the scattered intensity throughout the reciprocal space by sample (detector) scans at a fixed detector (sample) position. Some examples of the sample scans for as-deposited and laser treated Ag_4Co_1 and Ag_6Co_1 MLs are shown in Fig.4.The central ridge is specular XRR broadened by the experimental resolution function and ML mosaicity while the broad background (diffuse scattering) is due solely to the real (geometrical) interface roughness. Different frequency components of this roughness cause the wave vector transfer into different angles out of the specular direction.The diffuse scattering was simulated within the distorted-wave Born approximation (DWBA) to extract the parameters of the interface morphology and interface replication across the ML stack. The details of the calculations are described in Ref. 8. We used the lateral (self) correlation function of the type

$$C(x) = s_r^2 e^{-\left(\frac{x}{x}\right)^{2h}} \qquad (1)$$

for all interfaces where s_r, x, x, h stand for the root-mean-square (rms) value of real interface roughness, lateral distance, lateral correlation length and fractal parameter, respectively, the last being related to the fractal dimension of an interface as D=3-h.

In our case, h=1 for all samples so that fractal and topological interface dimensions are the same. This finding means that the interface profiles vary rather smoothly in lateral direction and no jaggedness typical for fractal behaviour occurs. Further, the vertical replication of the interface profiles was included in the simulations by a vertical (cross) correlation function expressed by an attenuation of the lateral correlation function according to the function[9] where z_j is the vertical (perpendicular to the interfaces) coordinate of the mean jth interface and L_{vert} is the vertical correlation length (L_{vert}=0 $\Rightarrow$ no replication of the interface profiles, $L_{vert}\to\infty$ $\Rightarrow$ total replication). The parameters of the diffuse scattering simulations are given in Table II. One can see that the interface morphology and its replication is changed considerably in laser treated Ag_6Co_1 ML only.

$$L(z_j - z_k) = e^{-\frac{|z_j - z_k|}{L_{vert}}} \qquad (2)$$

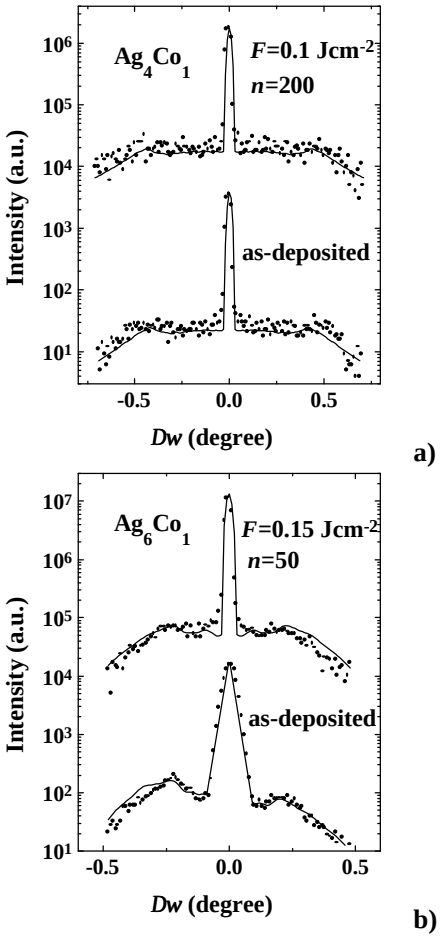

Fig. 4. Sample scans for (a) Ag_4Co_1 and (b) Ag_6Co_1 MLs before and after a laser irradiation. The measured curves (dots) were simulated within distorted-wave Born approximation (line) and for laser treated samples they are shifted upwards. *Dw* means the offset from the specular position. The detector was fixed at the positions shown in XRR curves (Fig.3) by the arrows.

TABLE I. Evolution of ML parameters with laser annealing obtained from the specular XRR simulations. *N, F, n, F_D, d, D, s* stand for the number of periods, fluence, number of pulses, deposited energy, individual layer thickness, ML period, and interface roughness, respectively. The layer thickness fluctuations included in the simulations reach 3-5 %.

sample	*N*	*F* (Jcm^{-2})	*n*	F_D (Jcm^{-2})	d_{Ag} (nm)	d_{Co} (nm)	*D* (nm)	*s* (nm)
Ag_2Co_1	5	0	0	0	2.1	1.2	3.3	0.9
		0.15	1	0.15	1.8	1.4	3.2	1.4
Ag_4Co_1	10	0	0	0	4.7	1.1	5.8	0.6
		0.1	200	20	4.65	1.0	5.65	0.6
		0.15	10	1.5	4.4	1.1	5.5	1.0
			20	3	4.4	1.1	5.5	1.1
			200	30	3.5	1.8	5.3	1.8
Ag_6Co_1	5	0	0	0	5.5	1.2	6.7	1.1
		0.15	10	1.5	5.2	1.6	6.8	1.2
			50	7.5	4.65	2.0	6.65	1.3
			100	15	4.0	2.5	6.5	1.3

4. Discussion

From our previous GMR measurements[1,2] it follows that for Ag_2Co_1 ML, there is little possibility to change the GMR systematically with laser treatment. Ag layers start melting already for F=0.15 Jcm^{-2} and no systematic change of the GMR occurs. For example, the original GMR of 11.5 % increases to 14.4 % for n=1 and then decreases to 2.5 % for n=100 at F=0.15 Jcm^{-2}. For F=0.2 Jcm^{-2}, the GMR reaches 7.6 % and 9.3 % for n=5 and n=20, respectively. The changes of the GMR ratio for Ag_4Co_1 ML are also not systematic but they are confined to a narrower interval around the original value even when the melting starts.. For example, the original GMR of 5.8 % decreases to 4.7 % both for n=1 and n=20 at F=0.15 Jcm^{-2}.

For Ag_6Co_1 ML, the original GMR increases systematically with the deposited energy in the irradiation regime without melting, i.e. up to F=0.2 Jcm^{-2}, being e.g. nearly doubled for n=20 at this fluence (13.5 %).

As the GMR effect originates from the spin-dependent interface electron scattering, its increase is determined by an increase of the interfacial area between non-magnetic and magnetic components. From this point of view, the breaking up of thin Co layers and formation of a discontinuous ML may explain the systematic GMR increase. In the following, we will inspect this point in more detail.

TABLE 2. ML parameters obtained from the simulations of the X-ray diffuse scattering at grazing incidence. s_r, x, L_{vert}, *and* h stand for the rms value of real (geometrical) interface roughness, lateral correlation length, vertical correlation length, and fractal parameter, respectively.

sample	*F* (Jcm^{-2})	*n*	F_D (Jcm^{-2})	s_r (nm)	x (nm)	L_{vert} (nm)	h
Ag_4Co_1	0.1	0	0	0.6	60	58	1
		200	20	0.6	60	56.5	1
Ag_6Co_1	0.15	0	0	1.1	50	33	1
		50	7.5	1.3	10	1	1

Laser treatment of Ag_6Co_1 ML below the melting threshold is connected with a decrease of Ag layer thicknesses while opposite is the case for Co layers, the ML period being generally reduced (Table I.). An enhanced decrement of the refractive index of Co layers in comparison with the theoretical one (by ≈10%) had to be taken into account in the XRR simulations.

These facts imply that Co layers are broken by Ag atoms penetrating between Co grains. Owing to the immiscibility of Ag and Co, grain boundary diffusion is the most probable mechanism. It can be seen that the thickness of such discontinuous Co layers is somewhat larger than in as-deposited state while Ag layers are gradually consumed. The ML character of the structure below the melting threshold is preserved.This ML evolution explains a systematic increase of the GMR with proceeding laser treatment of Ag_6Co_1 ML observed in Ref. 1,2. Ag_2Co_1 ML has a similar atomic structure of Ag layers as Ag_6Co_1 but a substantially narrower temperature window for a thermally driven diffusion process in solid state. Ag_2Co_1 ML is heavily disturbed already after F=0.15 Jcm^{-2} and n=1 irradiation when the melting of rather thin Ag layers starts.

The increase of the Co layer thicknesses at the expense of the Ag ones and increased interface roughness hint at the mixing of liquid Ag/solid Co interfaces which prevents from the formation of a discontinuous ML.

A highly non-equilibrium process of melting and rapid solidification on each laser pulse results into a recrystallized structure composed of Ag and Co granules (clusters) the parameters of which cannot be controlled in a predictable way. These parameters like number, sizes, shapes and distribution of Co clusters determine the GMR value. Consequently, the GMR evolution on laser treatment is not systematic for Ag_2Co_1 ML.

The reduction of the Ag layer thicknesses in Ag_4Co_1 ML for F=0.1 Jcm^{-2} irradiation is not accompanied by an increase of the Co layer thicknesses and may be ascribed to the annealing-out of defects in Ag layers. The satellites around 111 diffraction of fcc Ag persist up to F=0.15 Jcm^{-2} and n=20 irradiation.

Therefore, not only ML structure evidenced by the XRR but also its superlattice-like character is preserved. The strong texture obviously stabilizes the original structure even when melting starts. Only for F=0.15 Jcm^{-2} and n=200 irradiation, the texture is suppressed and the formation of a granular-like structure starts, similarly as in Ag_2Co_1 ML. Up to this point, the GMR of Ag_4Co_1 ML changes non-systematically but much less than for Ag_2Co_1 ML.

Owing to the immiscibility of Ag and Co, the interface morphology is fully controlled by the crystalline grains inside the layers. This conclusion is supported by the fact that the interface roughness s determined from the XRR simulations is equal to the real (geometrical) one s_r obtained from the GIDS simulations for all samples. Thus any change of the interface correlation is closely related to the grain morphology and size evolution induced by laser treatment. For Ag_6Co_1 ML, the vertical correlation length, comparable with the total ML thickness in as-deposited state, decreases to the level of Co layer thickness for F=0.15 Jcm^{-2} and n=50 irradiation (Table II.).

This means that grain boundary diffusion breaks the replication of interface profiles completely. Simultaneously, the lateral correlation length decreases 5 times which hints at the formation of smaller grains in discontinuous ML that promotes the GMR ratio. A small value of interface roughness in as-deposited Ag_4Co_1 ML is due to the brick-like shaped and nearly parallelly ordered Ag grains observed by cross sectional transmission electron microscopy[2].

The value of such small interface roughness is probably controlled by perfection of the grain connections rather than by the grains themselves. Contrary to Ag_6Co_1 ML, the vertical and lateral correlation lengths of interface profiles are little affected by laser treatment.

According to our recent studies of Co/Ag/Co trilayers[10], the diffusion coefficient of Ag in Co below 1000 K is $3x10^{-8}$ cm^{2}s^{-1}. The diffusion lengths calculated for this value and the pulse duration of 30 ns are at the level of the Co layer thickness or larger for n≥20. Therefore, a complete penetration of Co layers by Ag atoms leading to a discontinuous ML is principally possible. We also found a low activation energy which is typical for grain boundary diffusion, namely 0.38 eV[10].

Finally, the temperature dependences of magnetization measured at 10 Oe from 4.2 K up to room temperature with zero field cooling and field cooling reported in Ref. 2 give another evidence of the formation of a discontinuous ML in Ag_6Co_1. The difference at low temperatures between both curves increases after F=0.15 Jcm^{-2} and n=200 irradiation which indicates the presence of a granular-like component[11].

5. Conclusions

The behaviour of the GMR in Ag/Co MLs after excimer laser irradiation is closely related to the structural evolution which is determined by the atomic structure of the layers in as-deposited state as well as by the layer thicknesses. In Ag_6Co_1 ML with random polycrystalline structure, the GMR ratio increases systematically up to the melting threshold for Ag layers.

We have shown that the formation of a discontinuous ML, which takes place via grain boundary diffusion, is responsible for the GMR increase. Such a structure is in a way similar to that in granular thin films exhibiting the GMR effect. The formation of a discontinuous ML cannot be completed in Ag_2Co_1 ML where the temperature window for diffusion is too narrow. In Ag_4Co_1 ML, as-deposited structure is strongly textured which prevents from grain boundary diffusion of Ag into Co.Thus a controlled optimization of the GMR ratio is possible neither in Ag_2Co_1 nor Ag_4Co_1 MLs, though because of different reasons.

As soon as the melting threshold for Ag layers is reached, the ML structure is lost and a granular-like structure is established.

The parameters of this recrystallized structure, resulting from a highly non-equilibrium process, are rather random and have no link with the structure observed after laser annealing below the melting threshold. Thus a controlled optimization of the GMR is difficult.

Acknowledgements

The authors acknowledge a partial support by the Slovak scientific grant agency VEGA (project no. 5083/98) and by the Grant agency of the Czech Republic (project no. 101/98/0553). Some of the authors (M.J., A.A., E.M., M.S., Š.L., A.L., M.M.) acknowledge the support of NATO linkage grant no. HTECH.LG 971726

References

[1] Š. Luby, E. Majková, M. Spasova, M. Jergel, R. Senderák, E. D'Anna, A.Luches, M. Martino, M. Brunel, and I.M.Dmitrenko, Thin Sol. Films **312**, 15 (1998)..

[2] E. Majková, M. Spasova, M. Jergel, Š. Luby, S. Okayasu, A.Luches, M. Martino, E.N. Zubarev, and M. Brunel, Thin Sol. Films **343&344**, 211 (1999).

[3] J.D. Jarrat and J.A. Barnard, J. Appl. Phys. **79**, 5606 (1996).

[4] M. Iijima, Y. Shimizu, N. Kojima, A. Tanaka, and K. Kobayashi, J. Appl. Phys. **79**, 5602 (1996).

[5] Shi-Ming Zhou, Yu Wang,, Wei-Rong Zhu, Rong-Jun Zhang, Yu-Xiang Zheng, Quing-Yuan Jin, Liang-Yao Chen, Biao You, Wu Ji, An Hu, Hongru Zhai, and Honghi Shen, J. Appl. Phys. **83**, 900 (1998).

[6] E. D'Anna, S. Luby, A. Luches, E. Majkova, and M. Martino, Appl. Physics A **56**, 429 (1993).

[7] J.H. Underwood and T.W. Barbee Jr., AIP Conf. Proc. **75**, 170 (1981).

[8] M. Jergel, V. Holý, E. Majková, Š. Luby, R.Senderák, H.J.Stock, D.Menke, U.Kleineberg, and U.Heinzmann, Physica B **253**, 28 (1998).

[9] Z.H. Ming, A. Krol, Y.L. Soo, H. Kao, J.S. Park, and K.L. Wang, Phys. Rev. B **47**, 16373 (1993).

[10] E. D.'Anna, G. Leggieri, A. Luches, M. Martino, G. Majni, G. Barucca, P. Mengucci, Š. Luby, E. Majková, and M. Jergel, Thin Sol. Films **343&344**, 203 (1999).

[11] K. Honda, H. Sato, Y. Aoki, and S. Araki, J. Phys. Soc. Jpn. **64**, 2191 (1995).